Vertically downward gas-liquid flow: void fraction and pressure drop

Hiba Bouyahiaoui[1], Faiza Saidj[1], Abderraouf Arabi[2], Abdelsalam Al-Sarkhi[3], Abdelwahid Azzi[1*]

[1] LTPMP/FGMGP, Université des Sciences et de la Technologie Houari Boumediène, B.P 32 El Alia, Bab Ezzouar, Algiers 16111, Algeria

[2] Departament d'Enginyeria Mecànica, Universitat Rovira i Virgili, Av. Països Catalans 26, 43007, Tarragona, Spain

[3] Department of Mechanical Engineering, Center for Integrated Petroleum Research, King Fahd University of Petroleum and Minerals, Dhahran 31261, Saudi Arabia

*Corresponding author: Abdelwahid Azzi, E-mail: aazzi@usthb.dz Tel: +(213) 771 45 89 26

Abstract

Using an air-water mixture and 34 mm ID pipe, a series of pressure drop and void fraction measurements were collected. The observed flow regimes were falling film, annular, bubbly, cap bubble, slug, and churn flows. The temporal fluctuations of void fraction and pressure drop measurements were firstly studied using signals visualization and PDF. It was revealed that both signals can be used to identify the flow regimes. A new flow pattern map is proposed based on the Froude number, calculated using the mixture velocity of the two phases, and the ratio of gas-to-liquid superficial velocities. The behaviors of the total and frictional pressure drops were studied and the influence of the superficial velocities as well as the flow regimes were identified. The experimental results were compared to four existing vertically downward frictional pressure drop models, none of which provided accurate predictions.

Keywords: Gas-liquid, two-phase flow, vertical downward flow; void fraction, frictional pressure drop, flow regime, time series fluctuation

1 Introduction

Two-phase gas-liquid flows can be seen in many industrial applications. One can cite gas-oil production and transportation systems, nuclear and power plants, petrochemical industry, etc.

A simple examination of existing literature related to gas-liquid flow shows that the majority of the works carried out for the vertical upward and horizontal configuration, while less effort has been made for the vertical downward configuration which is the topic of this paper.

Recently, several applications need further investigation related to the downward two-phase flow configurations, for example: the simultaneous injection of water and gas for reservoir pressure maintenance (Hernandez et al., 2002) or Microbial Enhanced Oil Recovery (MEOR) (Xue et al., 2013) in petroleum production and exploitation, the plate-type nuclear fuel of research reactors (Chalgeri et al., 2022), the injection of CO_2 for CO_2 capture and storage (CCS) applications (Hammer et al., 2021), or its utilization in cooling systems in the context of the utilization of latter as a working medium with low Global Warming potential (GWP) (Schmidt et al., 2022).

A review of the gas-liquid flows in a vertical downward configuration literature shows that there is not a complete agreement on the classification of flow regimes in this configuration. Barnea et al. (1982), observed three flow regimes in 25 and 51 mm ID pipes, namely, dispersed bubbles, slug, and annular. Based on the fact that annular flow is the natural flow for this geometry, the authors used this regime to model the transition between the other regimes. Later, Usui (1989) introduced the falling film regime in his work. Moreover, the theoretical model of Lee et al. (2008) is based on the four regimes defined by Usui (1989). Some authors, such as Usui and Sato (1989), described the existence of six flow patterns, namely, bubbly, slug, cap bubble, churn, annular, and falling film.

Table 1 presents the existing flow pattern maps in literature. These maps are presented in 2D coordinates. Most of the published flow pattern maps are presented using the superficial gas

and liquid velocities for the *x* and *y*- coordinates. However, Yamazaki and Yamaguchi (1979) and Lau and Rezkallah (1995) proposed two flow pattern maps using two different coordinates.

Accurate estimation of pressure drop and gas void fraction are very crucial in many industrial applications. Proper estimation of the pressure drop is important for designing and optimizing the required pumping power and the size and the cost of any pumping system (Lau and Rezkallah, 1995, Liu et al., 2022). Gas Void Fraction (GVF) is also very important for characterizing the gas-liquid flow, and it is used to calculate the average phase velocity as well as the mixture density and to estimate the gravitational pressure gradient.

The most apparent difficulty to identify the flow regimes visually is the subjectivity of the visual observations. To overcome this inconvenience, the temporal signals of hydrodynamic parameters have been used in the present work as a tool to study, detect and identify the flow regimes. The static pressure, differential static pressure, void fraction, liquid holdup and temperature time series are generally used for this purpose (Guo et al., 2021; Liu et al., 2021, 2023; Arabi et al., 2023). Indeed, each regime has its own flow behavior through time, which reflects on the evolution of the above-mentioned parameters through the behavior of the temporal fluctuations. The fluctuations of the hydrodynamic parameters have been used by many scholars in horizontal or vertical upward flow, unfortunately this is not the case for vertical downward flow.

Table 1. Summary of existing flow pattern maps in vertically downward gas-liquid flow

Authors	Used fluid	Pipe diameter (mm)	Coordinates	Flow regimes
Yamazaki and Yamaguchi (1979)	Air-water	25	$\dot{m}_g$ $\dot{m}_l$ U_M, β	Bubbly, slug, whispy annular, and annular
Lau and Rezkallah (1995)	Air-water	9.53	U_{gs}, U_{ls} $\sqrt{\frac{U_{gs}}{U_{ls}}}$, Fr_M	Bubble, slug, froth, falling-film and annular
Bhagwat et al. (2012)	Air-water	12.52	U_{gs}, U_{ls}	Bubble, slug, froth, falling film, and annular
Xue et al. (2013)	Air-water	65	U_{gs}, U_{ls}	Bubble, slug, and churn
Qiao et al. (2017)	Air-water	50.8	U_{gs}, U_{ls}	Bubbly, Slug, churn-turbulent and annular
Bhagwat and Ghajar (2017)	Air-water	12.5	Re_{gs}, Re_{ls}	Annular, falling film, bubbly, slug, intermittent and transient
Kim et al. (2018)	Air-water	2.35 x 66.6 Rectangular section	U_{gs}, U_{ls}	Bubbly, Large bubbly, Cap bubble, Slug, Churn-turbulent, Falling film, Annular and Intermediate
Li et al. (2018)	Air-water	203.2	U_{gs}, U_{ls}	Cap bubbly, churn-turbulent and annular
Hammer et al. (2021)	CO_2	44	U_{gs}, U_{ls}	Annular, Annular-bubble, Cap bubble, Churn and Droplet
Schmidt et al. (2022)	CO2	8	G, x	Annular, bubbly, slug, and churn
Ghajar (2022)	Air-water	12.7	G_g, G_l	Bubbly, slug, intermittent, transient, falling film, and annular

Xue et al. (2013) analyzed the static pressure and pressure drop signals collected for bubbly, slug and churn flows in a 65 mm ID pipe. It was observed that both signals contain small amplitude with high-frequency fluctuations. The presence of a distinguishable peak was reported for slug flow whereas the latter disappeared with the transition to churn flow. Li et al. (2018) reported that the PDF calculated from time series of void fractions are different for cap bubbly, churn-turbulent and annular flows. Chalgeri and Jeong (2019) collected void fraction and differential pressure time series for the bubbly, large-bubbly, cap-bubbly, slug, churn-turbulent, annular, and falling film. The void fraction time series have given more sensitivity to detect the large-bubbly flow. The authors proposed the PDF obtained with void fraction time series as a tool to detect the flow regimes. It is important to note that only few papers focused on studying of the difference between pressure drop and void fraction time series. By comparing the PDF obtained with both kinds of signal in the case of air-silicone oil two-phase flow vertical upward flow, Abdulkadir et al. (2020) reported that the PDF signatures are different for slug flow.

In addition to the visual identification of the flow regimes and their range of existence, some investigators have focused on the study of the hydrodynamic behavior of specific flow regime. This is was done for the bubbly flow (Ishii et al., 2004), annular flow (Hajiloo et al., 2001; Santana et al., 2021; Voulgaropoulos et al., 2021, Cherdantsev et al., 2021), and slug flow (Bouyahiaoui et al, 2018). The latter has generated a database of hydrodynamic parameters of the slug flow, which are used as input parameters in predictive models used in the oil & gas industry.

Due to the lack of enough knowledge on the vertical downward flow, in comparison with vertical upward flow, some studies have made a comparison between the flow behavior in these two geometric configurations in order to identify some analogies between both flows. Bouyahiaoui et al. (2020) used the void fraction time series obtained using water-air mixture in

34 mm ID pipe to perform a comparison between the behavior of several parameters between upward and downward configurations for churn flow regime. It was found different values of distribution coefficient, C_0, from drift flux analyses. Using the slippage number, introduced by Al-Sarkhi et al. (2016b), the authors reported that the behavior of the churn flow for both configurations is different for a mixture Froude number less than 4. Indeed, the slippage number has positive and negative values for upward and downward flows, respectively. The negative values of the slippage number mean that the void fraction is higher than the homogenous void fraction. The plot of the structure velocities obtained in both cases has shown that this parameter is more dependent on the mixture velocity in the upward flow compared to that in the downward flow.

Hammer et al. (2021) generated a database of liquid holdup and frictional pressure drop for upward and downward vertical flow using CO_2 as a working fluid. After comparing the predictions of several existing models of these two parameters, the authors reported that the values of the void fraction are practically the same for both directions. The frictional pressure drop recorded in the upward configuration is found to be higher than those recorded in the vertical downward configuration.

More recently, Abdulkadir et al. (2021) also performed a comparison between hydrodynamic parameters in the case of upward and downward. The study was carried out with an air-water mixture in a 127 mm pipe and using ring probes for liquid holdup measurement. In both configurations, a total of 85 acquisitions of liquid holdup signals, corresponding to the same flow conditions of both phases, were collected. The churn and annular regimes were observed in the upward configuration, while only the latter was reported in the second geometry. They reported that the coefficient C_0 in the case of a downward direction is higher than that found in the upward direction. The experimental results of void fraction were also compared with some existing models.

The results obtained by the three above-mentioned works allow us to understand that the behavior of frictional pressure drop and void fraction are different for upward and downward flows. Thus, the results obtained with the vertical upward flow cannot be extrapolated to the vertically downward flow. The few works carried out for this flow configuration, compared to the vertical upward flow, highlights the necessity to carry out further experimental investigations and to generate additional databases to advance our knowledge for this geometrical configuration. The database collected can also be used to validate the numerical simulations obtained using Computational Fluid Dynamics (CFD) (Kang et al., 2021; Passoni et al., 2023).

Concerning the studies devoted to the total and frictional pressure drop, Friedel (1979) has stated that there is no study where the frictional pressure drop models are evaluated in the case of vertical downward flow. He has also explained that the influence of the flow regime on the pressure drop, in all pipe orientations, is not yet quantifiable. Using a database, the author proposed two predictive models. The first is devoted to vertical upward and horizontal configurations, while the second is specific to vertical downward flow. The latter is based on 1311 experimental data points. The fact that the author proposed a specific model for vertical downward flow shows the specificity of this configuration, compared to the two other configurations. After extensive literature review, we have enumerated only four models (Yamazaki and Yamaguchi, 1979; Friedel, 1979; Yao et al., 2016 and Lu et al., 2018) built specifically for vertical downward flow.

Using air-water in a 65 mm ID pipe, Xue et al. (2013) investigated the pressure drop for gas-liquid two-phase flow downward vertical pipe. It was reported that the transition of the slug-to-churn flow has induced a variation of the trend of the frictional pressure drop as a function of the gas superficial velocity. It is important to note that the authors didn’t measure the void fraction, so they calculated the gravitational pressure drop by using a void fraction model of

Goda et al. (2003). Bhagwat et al. (2012) and Yao et al. (2016) have also noted that the evolution of the frictional pressure drop depends on the nature of the flow regime. These two studies also evaluated the predictions of existing models, including that developed for vertical upward and horizontal flow. Lu et al. (2018) pointed out the lack of existing data in the case of moderate (10 > ID > 100 mm) and large (ID > 100 mm) pipe diameters. Their data generated using a 50.8 mm ID were compared with some existing models and a novel correlation based on the Lockhart-Martinelli approach was proposed. It is noted that the models developed for vertical downward flow have not been evaluated by the authors.

In light of the presented detailed review of the available literature on researches carried out on downward vertical gas-liquid flows, it is clearly observed that the scarcity of studies carried out as well as the limited existing database for void fraction and pressure drop, compared to other geometrical configurations. In addition, it is realized that the knowledge acquired on vertical upward flow cannot be directly extrapolated to the vertically downward flow. The present work aims to fill this gap through generation of a novel experimental database for the two parameters (void fraction and pressure drop) using a mixture of air-water flowing in a 34 mm pipe covering six flow regimes namely bubbly, cap bubble, slug, churn, annular and falling film regimes. The behavior of both parameters, mean values and time series evolution, for each regime will be investigated in the present paper. Moreover, an evaluation of the available predictive models of frictional pressure drop for downward flow will be presented in this paper.

2 Existing two-phase frictional pressure drop models for vertical downward two-phase flow

In this section, the existing models to predict the frictional pressure drop, $\left(\frac{dP}{dL}\right)_{f,TP}$, for the vertical downward two-phase flow will be discussed. The total pressure drop is the sum of the frictional, gravitational, and acceleration pressure drops, and given by (Eq. 1).

$$\left(\frac{dP}{dL}\right)_{TP} = \left(\frac{dP}{dL}\right)_{f,TP} + \left(\frac{dP}{dL}\right)_{a,TP} + \left(\frac{dP}{dL}\right)_{g,TP} \quad (1)$$

where $\left(\frac{dP}{dL}\right)_{f,TP}$ is the two-phase friction pressure gradient, $\left(\frac{dP}{dz}\right)_{a,TP}$ the pressure gradient due to the contraction or expansion of gas-phase as the two phases travel along the test section is given by Eq. 2:

$$\left(\frac{\mathrm{d}P}{\mathrm{d}L}\right)_{a,TP} = \frac{d}{dz}\left(\frac{G_l^2}{\varepsilon_g \rho_l} + \frac{G_g^2}{(1-\varepsilon_g)\rho_g}\right) \quad (2)$$

with G is the mass flux. The indices l and g denote liquid and gas phase, respectively and ε_g is the void fraction.

$\left(\frac{dP}{dL}\right)_{g,TP}$ is the pressure gradient due to the gravity, calculated by:

$$\left(\frac{dP}{dL}\right)_{g,TP} = \rho_{TP} g sin\theta \quad (3)$$

ρ_{TP}, g, and θ are the gas-liquid mixture density, gravity, and pipe inclination, respectively. The density of the gas-liquid mixture is given by Eq. 4.

$$\rho_{TP} = \varepsilon_g \rho_g + (1-\varepsilon_g)\rho_l \quad (4)$$

The acceleration pressure drop term is generally neglected in the case of non-boiling two-phase flow (Lu et al., 2018).

Regarding the frictional pressure drop, the existing vertical downward models are all based on the heterogeneous flow assumption where the slip between the two phases is considered. In this approach, the frictional pressure drop is the product of the liquid frictional pressure gradient, $\left(\frac{dP}{dL}\right)_l$, or only liquid frictional pressure gradient, $\left(\frac{dP}{dL}\right)_{lo}$, and the two-phase frictional multiplier, ϕ_l^2 or ϕ_{lo}^2, as in Eqs. 5 and 6, respectively.

$$\left(\frac{dP}{dL}\right)_{f,TP} = \phi_l^2 \left(\frac{dP}{dL}\right)_l \tag{5}$$

$$\left(\frac{dP}{dL}\right)_{f,TP} = \phi_{lo}^2 \left(\frac{dP}{dL}\right)_{lo} \tag{6}$$

The indices *l* and *lo* refer to liquid and liquid only, respectively. In the former case, the liquid flow rate is assumed; while the two-phase mixture mass flux, G_{TP} is used in lo case. The pressure drop in both cases are expressed as:

$$\left(\frac{dP}{dL}\right)_l = \frac{f_l G_l^2}{2D\rho_l} \tag{7}$$

$$\left(\frac{dP}{dL}\right)_{lo} = \frac{f_{lo} G_{TP}^2}{2D\rho_l} \tag{8}$$

where f_l and f_{lo} designate the Darcy-Weisbach friction factor for the *l* and *lo* case given respectively by Eqs. 9 and 10. Noting that for turbulent flow, we have considered the correlation of Fang et al. (2011).

$$f_l = \begin{cases} 64/Re_l \text{ for laminar flow} \\ 0.25\left[log\left(\frac{150.39}{Re_l^{0.98865}} - \frac{152.66}{Re_l}\right)\right]^{-2} \text{ for turbulent flow} \end{cases} \tag{9}$$

$$f_{lo} = \begin{cases} 64/Re_{lO} \text{ for laminar flow} \\ 0.25\left[log\left(\frac{150.39}{Re_{l0}^{0.98865}} - \frac{152.66}{Re_{l0}}\right)\right]^{-2} \text{ for turbulent flow} \end{cases} \quad (10)$$

Based on the lack of agreement in the literature regarding the Reynolds number at which the transition from laminar flow to turbulent flow occurs, we have selected a critical value of *Re* = 1055 to distinguish between viscous and turbulent flows. This value corresponds to the intersection of the curves for laminar and turbulent flows, as depicted in Fig 1.

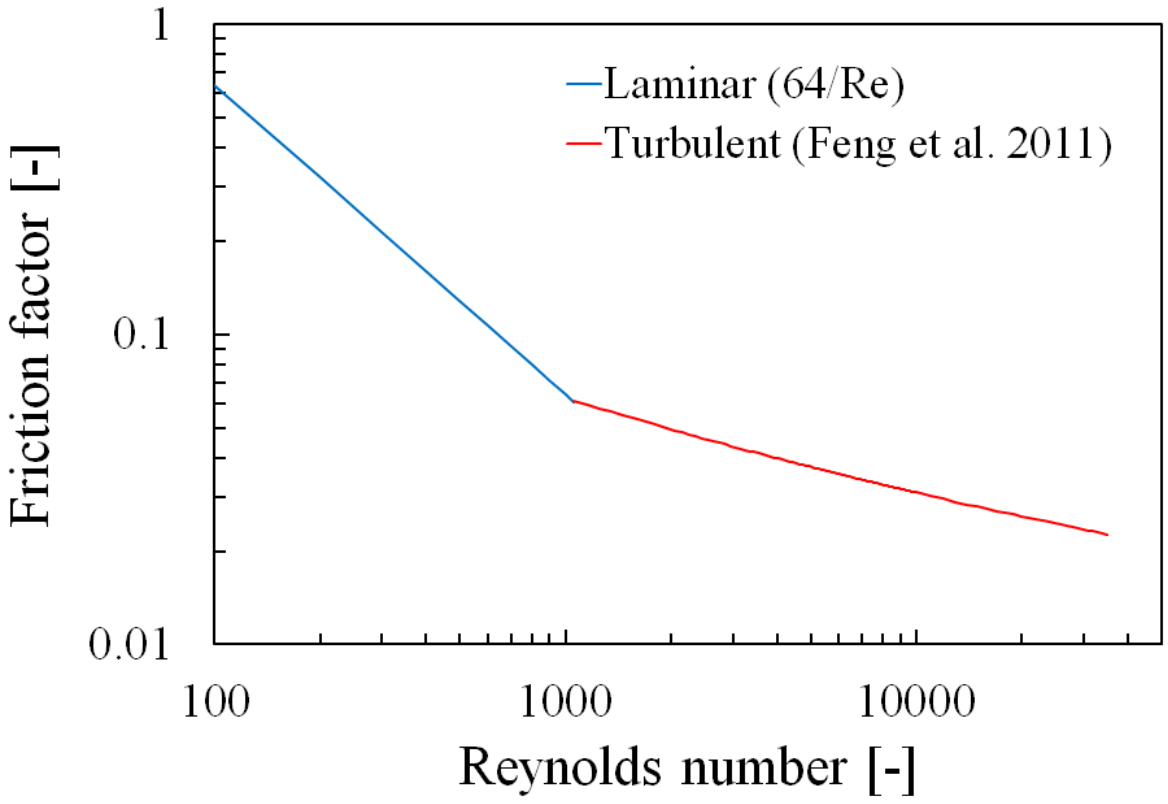

Fig. 1. Representation of the evolution of Darcy-Weisbach friction factor in function of Reynolds number.

The Reynolds numbers for the case of liquid, Re_l, and liquid only Reynolds number, Re_{lo}, are calculated as follows:

$$Re_l = \frac{G_l D}{\mu_l} \tag{11}$$

$$Re_{lo} = \frac{G_{TP} D}{\mu_l} \tag{12}$$

For the estimation of the two-phase multipliers, different studies have proposed different correlations depending on the used database and on the significant parameters. These formulas are summarized in Table 2.

Table 2. Existing models for predicting gas-liquid downward frictional pressure drop

Authors	**Correlation**
Yamakazi and Yamaguchi (1979)	$\Phi_{lo} = (1-\varepsilon_g)^{-0.9}$
	$\frac{\varepsilon_g}{(1-\varepsilon_g)(1-K\varepsilon_g)} = \frac{\beta}{1-\beta}$
	$\beta = \frac{U_{gs}}{U_{gs}+U_{ls}}$
	$K = \begin{cases} 2 - 0.4/\beta \; for \; \beta \leq 0.2 \\ -0.25 + 1.25\beta \text{ for } \beta \geq 0.2 \end{cases}$
Friedel (1979)	$\Phi_{lo}^2 = (1-\dot{x})^2 + \dot{x}^2 \frac{\rho_l}{\rho_g}\frac{f_{go}}{f_{lo}} + \frac{48.6\dot{x}^{0.8}(1-\dot{x})^{0.29}\left(\frac{\rho_l}{\rho_g}\right)^{0.9}\left(\frac{\mu_g}{\mu_l}\right)^{0.73}\left(1-\frac{\mu_g}{\mu_l}\right)^{7.4} {Fr_F}^{0.03}}{We_F^{0.12}}$
	$\dot{x} = \frac{G_g}{G_{TP}}$
	$Fr_F = \frac{G_{TP}^2}{\rho_{TPH}^2 g D}$

	$$We_F = \frac{G_{TP}^2 D}{\rho_{TPH}\sigma}$$
	$$\rho_{TPH} = \left[\frac{\dot{x}}{\rho_g} + \frac{1-\dot{x}}{\rho_l}\right]^{-1}$$
	$$f_{lo} = \begin{cases} 64/Re_{lo} \text{ for laminar flow} \\ \left[0.86859 ln\left(\frac{Re_{lo}}{1.964Re_{lo} - 3.8215}\right)\right]^{-2} \text{ for turbulent flow} \end{cases}$$
	$$f_{go} = \begin{cases} 64/Re_{go} \text{ for laminar flow} \\ \left[0.86859 ln\left(\frac{Re_{go}}{1.964Re_{go} - 3.8215}\right)\right]^{-2} f\text{or turbulent flow} \end{cases}$$
Yao et al. (2018)	$$\phi_l^2 = 1 + \frac{C}{X} + \frac{1}{X^2} + B$$
	$$C = \begin{cases} 5\ for\ Re_g < 1055\ and\ Re_l < 1055 \\ 10\ for\ Re_g < 1055\ and\ Re_l \geq 1055 \\ 12\ for\ Re_g \geq 1055\ and\ Re_l < 1055 \\ 20\ for\ Re_g \geq 1055\ and\ Re_l \geq 1055 \end{cases}$$
	$$B = 36.371\left[\left(\frac{gD}{U_{ls}^2}\right)\left(1 - \frac{\rho_g}{\rho_l}\right)\right]^{1.278}\ 0.995^{\left[X - \left(\frac{\rho_l}{\rho_g}\right)^{-0.01}\left(\frac{\mu_l}{\mu_g}\right)^{0.77}\left(\frac{\sqrt{gD}}{U_{ls}}\right)^{0.41}\right]^2}$$
	$$X = \sqrt{\frac{\left(\frac{dP}{dL}\right)_l}{\left(\frac{dP}{dL}\right)_g}}$$
Lu et al. (2021)	$$\Phi_l^2 = 1 + \frac{50}{X} + \frac{1}{X^2}$$

3 Experimental facility and procedure

The experiments were conducted using air-water mixture flowing through a vertical 34 mm ID pipe. The experimental setup used previously by Bouyahiaoui et al. (2018, 2020) is displayed in Fig. 2. The pipe is made from transparent Perspex to allow flow visualization. It has a 4 mm

thickness, 34 mm internal diameter, and is 7.8 m length. The experiments have been performed at an ambient temperature of 25 °C. The properties of both phases are summarized in Table 3.

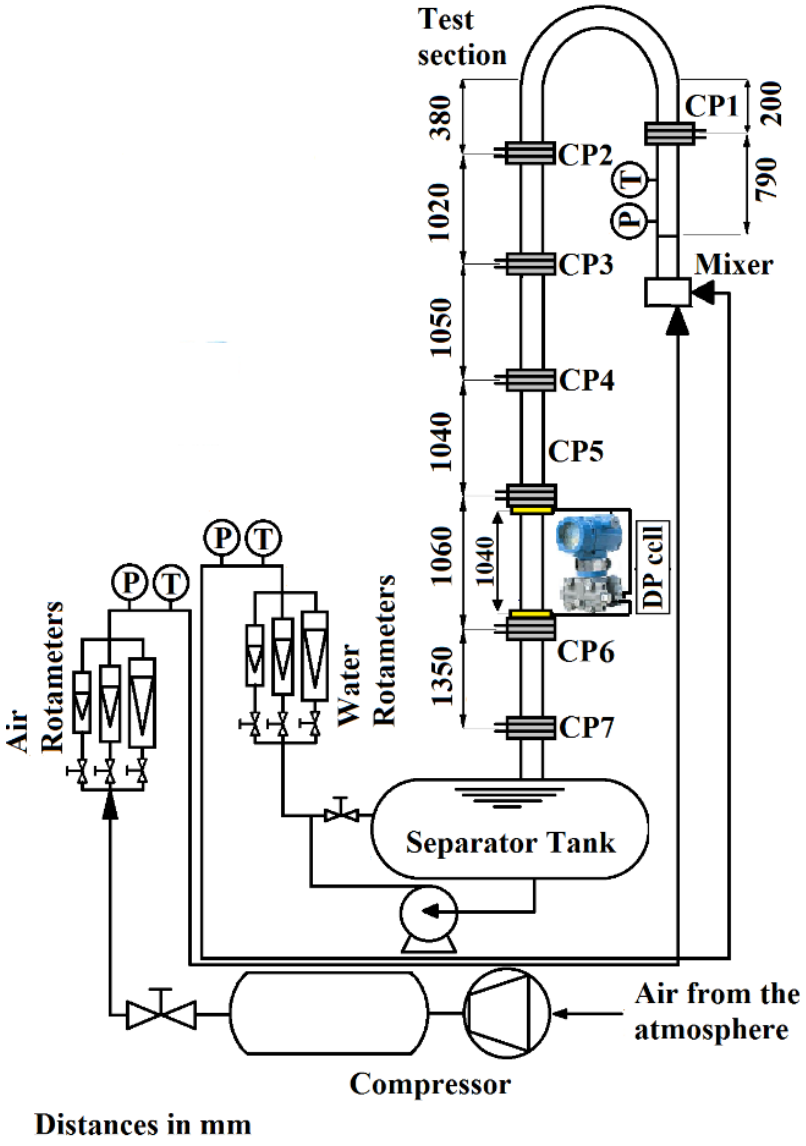

Fig. 2. Experimental facility Schematic.

Table 3. Considered air and water properties

Parameter	Water	Air
Density [Kg/m^3]	997.13	1.2119
Dynamic viscosity [Kg/m.s]	1.00×10^{-3}	1.185×10^{-5}
Surface tension [N/m]	0.072	

Water is pumped from a storage tank (separator) to the two-phase mixer. Water rotameters were placed within the water circuit to control the water flow rates up to a value of 4.5 m^3/h. Air from the atmosphere is drawn by a compressor to the mixing chamber and its flow rate is controlled by air rotameters in a range of 1 to 150 l/min. The accuracies of the gas and the liquid rotameters are within ± 2% of the full scale.

The mixing device consists of two Polyvinyl Chloride (PVC) pieces. The first piece is a cylindrical tube with an 80 mm diameter and 64 holes of 1 mm diameter. The gas phase is introduced through the holes in the mixing chamber, which is the annular space between the two pieces of the mixer. The liquid phase is then injected into the mixing chamber. The detail of this geometry can be found in Saidj et al. (2014).

The mixture of two phases moves upwards through a pipe that is 1 meter long. After that, the flow is reversed to move downwards by using an inverted U-bend. The flow then moves through the downward section of the test area which comprises a pipe that is about 6 meters length. Finally, the mixture is discharged into a storage tank where the two phases are separated.

It is also worth to be mentioned that the static pressure and temperature of the two phases were constantly checked, before being mixed using an absolute pressure transmitter with [0 – 1.6] bar range with a 0.1% accuracy on the full scale and a thermometer measuring values up to 100°C with a 1% accuracy on the full scale.

To determine the average void fraction across the cross-sectional area, seven probes were installed along the test section. The probes included CP1, which was positioned 6D upstream of the inverted U-bend, and CP2 to CP7 probes, which were installed at 11, 41, 72, 102, 134, and 173D downstream of the bend. These conductance probes were specifically made in-house to measure the void fraction. This technique works by measuring the electrical conductivity of the water and air. The relation between the medium's electrical impedance and the phase distribution was first derived, and then the cross-sectional averaged void fraction was obtained using this technique.

The probe consisted of two stainless steel electrodes, shaped like rings, which were placed inside a Plexiglas casing (see Fig. 3). The electrodes were 2 mm wide (referred as s) and spaced 12mm apart (referred as De). Bouyahiaoui (2019) provides further details on this technique.

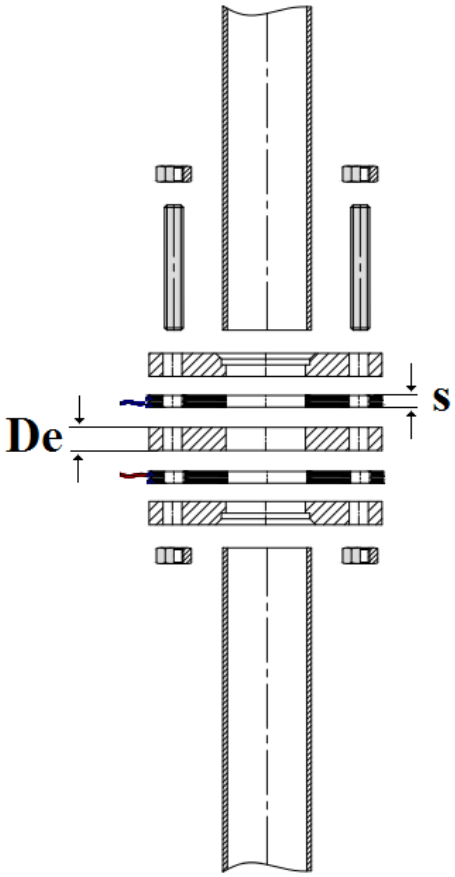

Fig. 3. Schematic diagram of the conductance probe.

The differential pressure drop was measured using differential pressure transmitters located between 3.5 m and 4.5 m downstream of the U-bend, where the two-phase flow is fully developed (Bouyahiaoui et al., 2018).

Figure 4.a shows the setup used for measuring differential pressure. To cover the entire range of pressure drop, two FOXOBORO transmitters were used, one at a time. The DP cell measuring [0 - 7.2 kPa] was used for low values, whereas the one measuring [0 - 36kPa] was used for high values. Both transmitters have an accuracy of 2% of their full scale. To prevent the penetration of the two-phase mixture into the pressure drop transmitters, which might generate over-estimated fluctuations in the recorded signals, a purging system was installed.

The purging system was previously discussed by Zeghloul et al. (2017). The two transmitters were calibrated by converting their output voltage into pressure. Fig 4.b shows the linear calibration curves obtained.

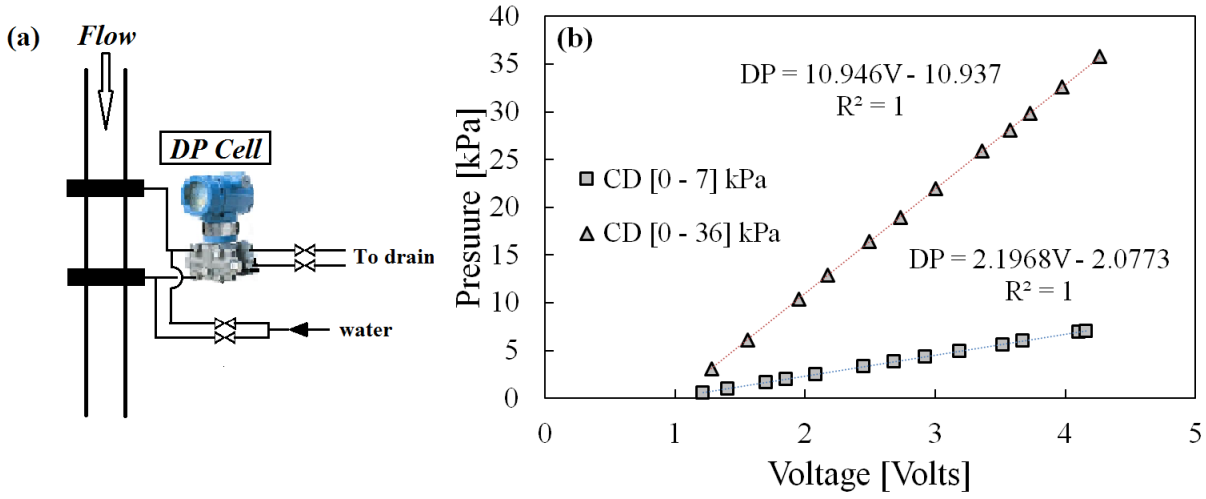

Fig. 4. Details of differential pressure transmitter system used (a) positioning in the pipe and (b) calibration curves.

The LabVIEW software by NIDAQ, 12 bit-6092E unit was used to acquire the experimental data from the conductance probe, temperature sensor, pressure, and differential pressure transmitters. For each run, signals of a duration of 60s was acquired at a sampling frequency of 200 Hz.

4. Results and Discussion

The present experiments consist of 194 data points corresponding to $0.019 \leq U_{gs} \leq 3.24$ m/s and $0.015 \leq U_{ls} \leq 1.40$ m/s. In these ranges of superficial velocities, six flow patterns were observed: falling film, annular, bubbly, cap bubble, slug and churn flows (see Fig. 5).

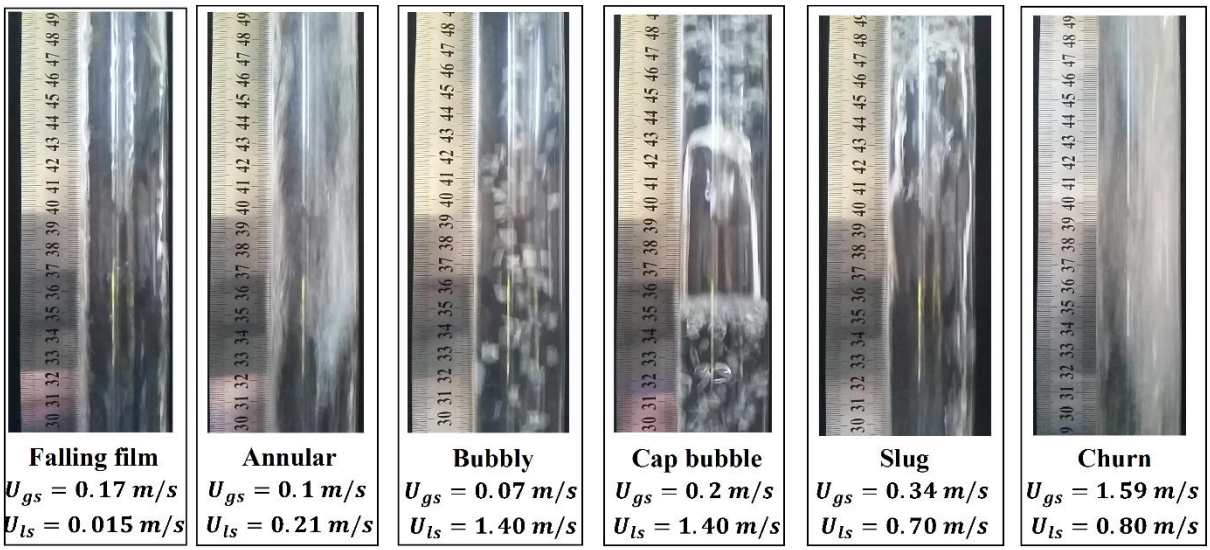

Fig. 5. Observed flow regimes in the present experiments.

4.1 Void fraction time series

It is worth noting that this paper only presents results obtained with CP 7. The void fraction obtained with CP 2 to CP 7 is solely used to ensure that the flow is fully developed at CP 7. The void fraction time traces of all flow regimes of the air water mixture in the 34 mm ID pipe are presented in Fig. 6.

The falling film flow was the first flow regime to appear in this study even at "zero" gas flow rate. Figure 6.a shows the void fraction time series of the falling film regime. The signal shows a consistently high void fraction, with a value exceeding 0.95. This is because the gas takes up the central core of the tube, leaving only a thin liquid film. The small fluctuations in the signal are caused by low-amplitude waves at the interface of the gas core and liquid film.

As the liquid flow rate increments, an increase in interfacial waves at the interface between the gas core and the liquid film occurs. This behavior is due to the transition to annular flow appearing in the void fraction time series, as shown in Fig. 6.b.

Bubbly flow only appears for very high liquid flow rates. Fig. 6.c shows that the lowest values of void fractions were recorded in this regime since the pipe was full of water with gas bubbles flowing downward along the tube.

An increase in gas flow rates creates larger bubbles with higher void fractions called cap bubbles. An example of the signal obtained with this flow regime is presented in Fig. 6.d. The transition to a cap bubble is due to the bubble's coalescence. The coalescence phenomenon of gas bubbles increases with the increase of gas superficial velocities.

The time series of slug flow (depicted in Fig. 6.e) displays the intermittent nature of this flow pattern, which affects the passage of Taylor Bubbles at a high void fraction and the liquid slug at a low void fraction. This flow pattern has been previously studied by Bouyahiaoui et al. (2018). The churn flow is observed at high gas flow rates, and the void fraction signal shows high mean void fractions with significant fluctuations caused by the breaking of Taylor bubbles.

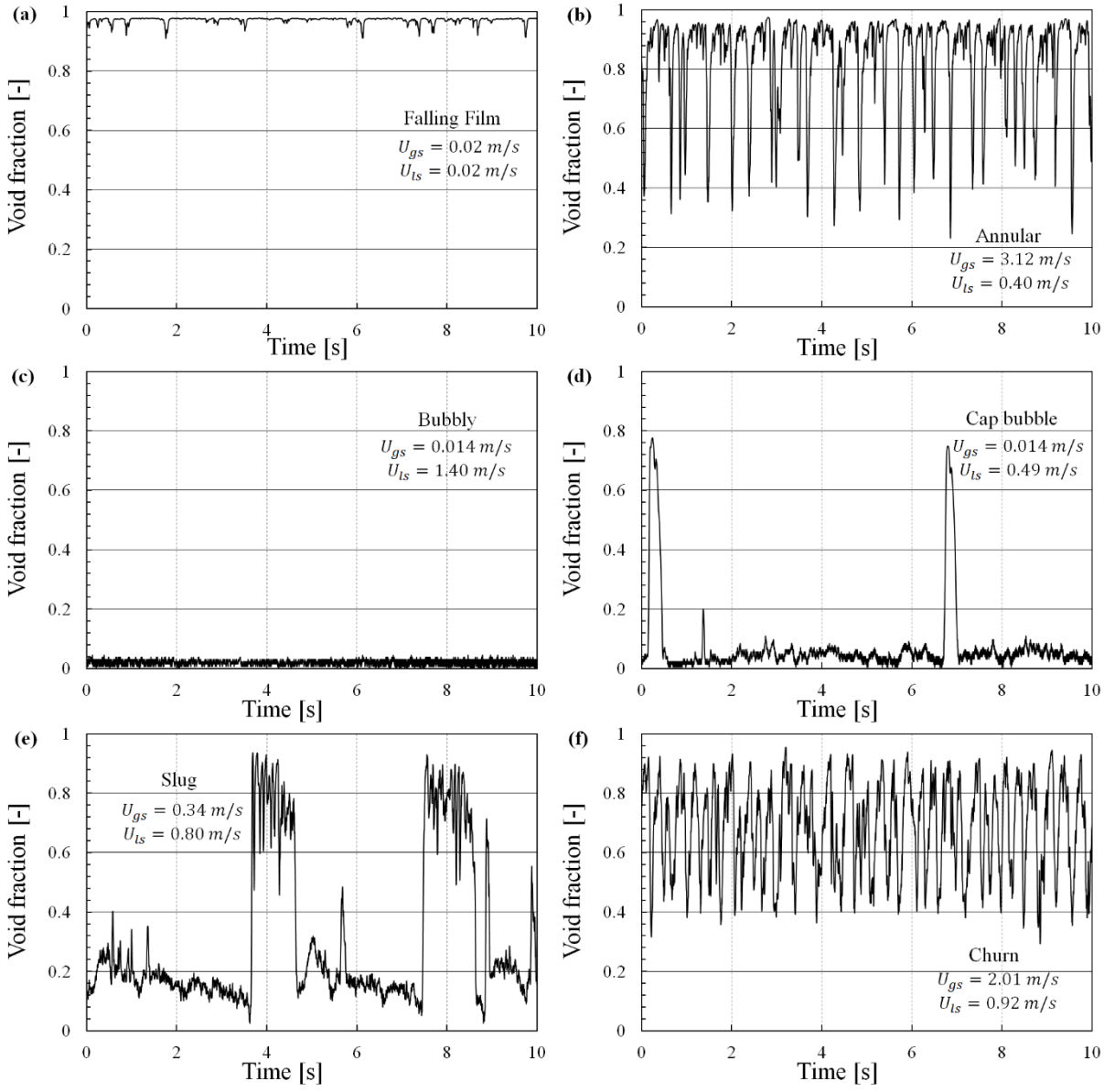

Fig. 6. Examples of Void fraction time series obtained for the six reported flow patterns.

4.2 Pressure drop time series

Figure 7 presents examples of pressure drop time series obtained for the six regimes observed in the current study. For superficial gas and liquid velocities of 0.02 m/s (Fig 7.a), falling film flow pattern takes place and it is characterised by a gas core and a liquid film falling sticking to the tube wall. The liquid film is constantly crossed by long waves with low amplitudes flowing

downward. Similar to the void fraction time series (Fig. 6.a), the pressure drop signal is relatively constant with the presence of small fluctuations. As the rates of liquid flow increase, the waves forming within the liquid film start to gain more amplitude and become more significant. This, in turn, leads to higher values of shear stress at the interface between the gas and liquid, which can cause small liquid droplets to tear apart.

Figure 7.b represents the pressure drop signal of a typical annular flow observed at $U_{gs} = 3.12\, m/s$ and $U_{ls} = 0.40\, m/s$. A detailed analysis reveals that annular flow experiences greater fluctuations than falling film flow, which was already discussed in by Zadrazil et al. (2014).

Increasing the superficial liquid velocity, the segregated flow with a clear separation of the two phases disappears, forming the bubbly and intermittent flows. This phenomenon appears on the signature of pressure drop signals, with the presence of important fluctuations. Bubbly flow is the hardest flow regime to get in the downward two-phase flow configuration. It is observed at high liquid rates and low gas rates. As shown in Fig. 7.c, the passage of dispersed gas bubbles inside the space between the two pressure taps is reflected by an increase in the pressure drop. As vertical upward flow (Arabi et al., 2022), the increase of gas superficial velocity induces the coalescence of the gas bubbles forming cap bubbles. The reduction in the fluctuation of pressure drop time series (shown in Fig. 7.d) is attributed to the fact that the number of cap bubbles is less than that of gas bubbles.

The time series collected with the slug flow is characterized by important fluctuations of the pressure drop (Fig. 7.e). This is due to the successive passage of liquid slugs and Taylor bubbles. These structures have tendency to vanish with the transition to churn flow (Bouyahiaoui et al., 2020). The increase in gas flow rates causes Taylor bubbles to break, resulting in a churn flow

pattern. The signal obtained with this kind of flow is relatively similar to the one obtained with the annular flow, except the presence of more important fluctuations (Fig. 7.f).

The reported shapes of pressure drop time series for the six flow regimes are similar to those reported for void fraction time series.

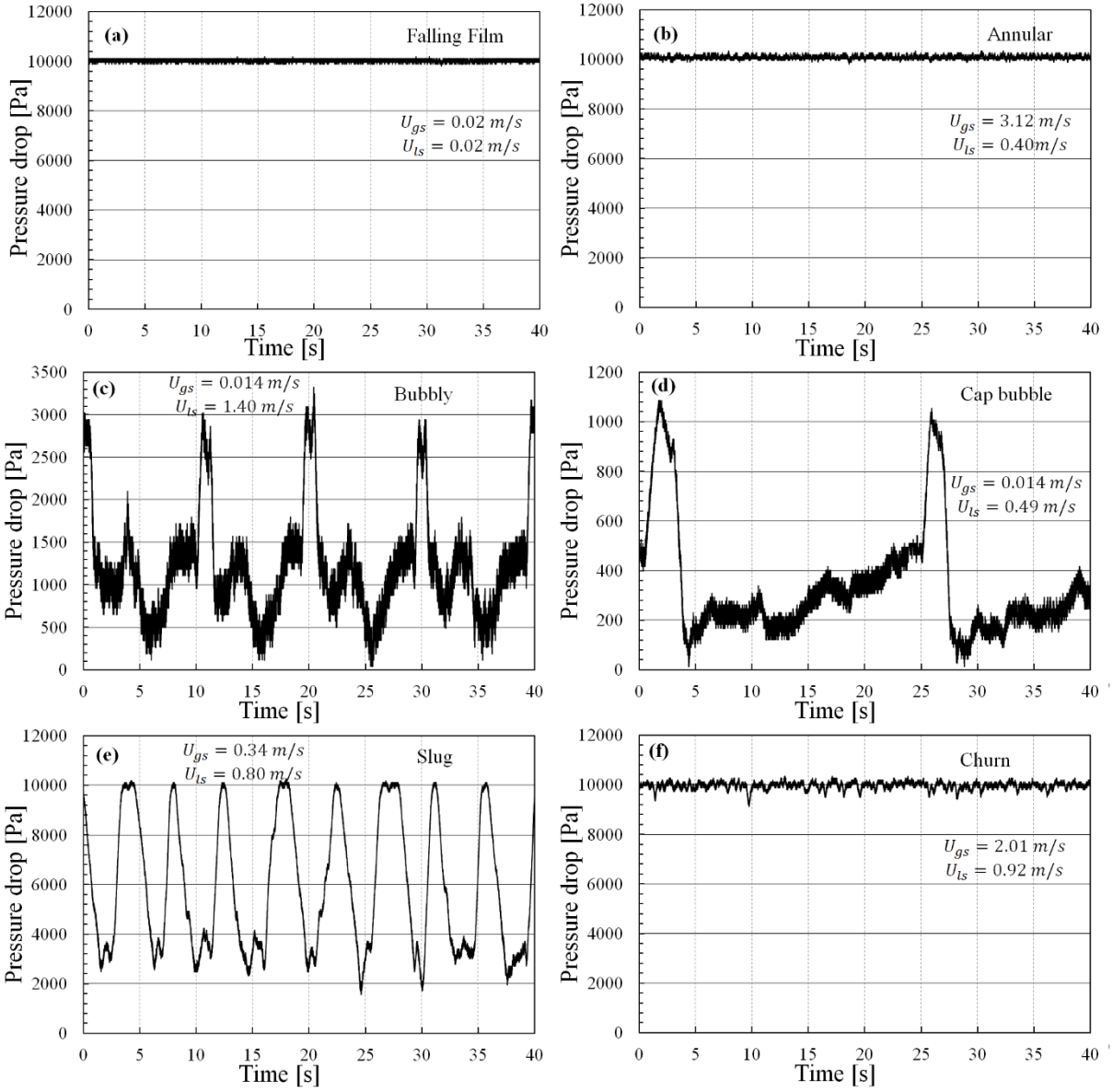

Fig. 7. Examples of pressure drop time series obtained for different flow patterns.

4.3 PDFs of void fraction and pressure drop time series

In addition to the void fraction time series, the Probability Density Function (PDF) of the pressure drop time series was calculated to identify the flow regimes. It is well known that the PDF obtained with the void fraction or liquid holdup signals is used for this purpose for vertical upward flow (Costigan and Whalley, 1997). In order to have signals values between 0 and 1, the pressure drop signals were normalized using the method proposed by Matsui (1984). Each value of the collected pressure drop of the signal (ΔP_i) is divided by the differential pressure of static liquid column in the corresponding measured section (ΔP_l) as follows:

$$\Delta P_i^* = \frac{\Delta P_i}{\Delta P_l} = \frac{\Delta P_i}{\rho_l g h} \tag{13}$$

with ΔP_i^* the normalized pressure drop and h the distance between the two pressure taps expressed in meter (1.04 m in the present study).

The PDF of the normalized pressure drop expressed in Eq. 13 as well as of the void fraction time series are plotted together in Fig. 8 for the six observed flow regimes.

It appears that the PDF of pressure drop of the falling film (Fig. 8.a), annular (Fig. 8.b), and churn (Fig. 8.f) are similar by the presence of a single peak at high values of normalized pressure drop. One peak at low normalized pressure drop values is exhibited by the PDF of bubbly and cap bubble flows, as shown in Fig. 8.c and 8.d, respectively. For slug flow (Fig. 8.e), two distinct peaks are observed. The peaks observed at high and low values of normalized pressure drop corresponds to the passage of the liquid slugs and Taylor bubbles, respectively.

There are some similarities between the PDF obtained from void fraction time series and those obtained from slug , bubbly, and cap bubble flows. However, the PDFs obtained from the latter signals enable the differentiation between falling film, annular, and churn flows.

Indeed, for the falling film regime, the PDF has a sharp and extremely narrow peak situated at a very high void fraction value; while the peak presents in the annular flow is larger than that of the falling film flow. In addition, it is positioned at lower void fraction value than that observed for the falling film regime. The churn flow generates multiple peaks of high sizes and more wrinkles on the PDF curve compared to the two previous patterns.

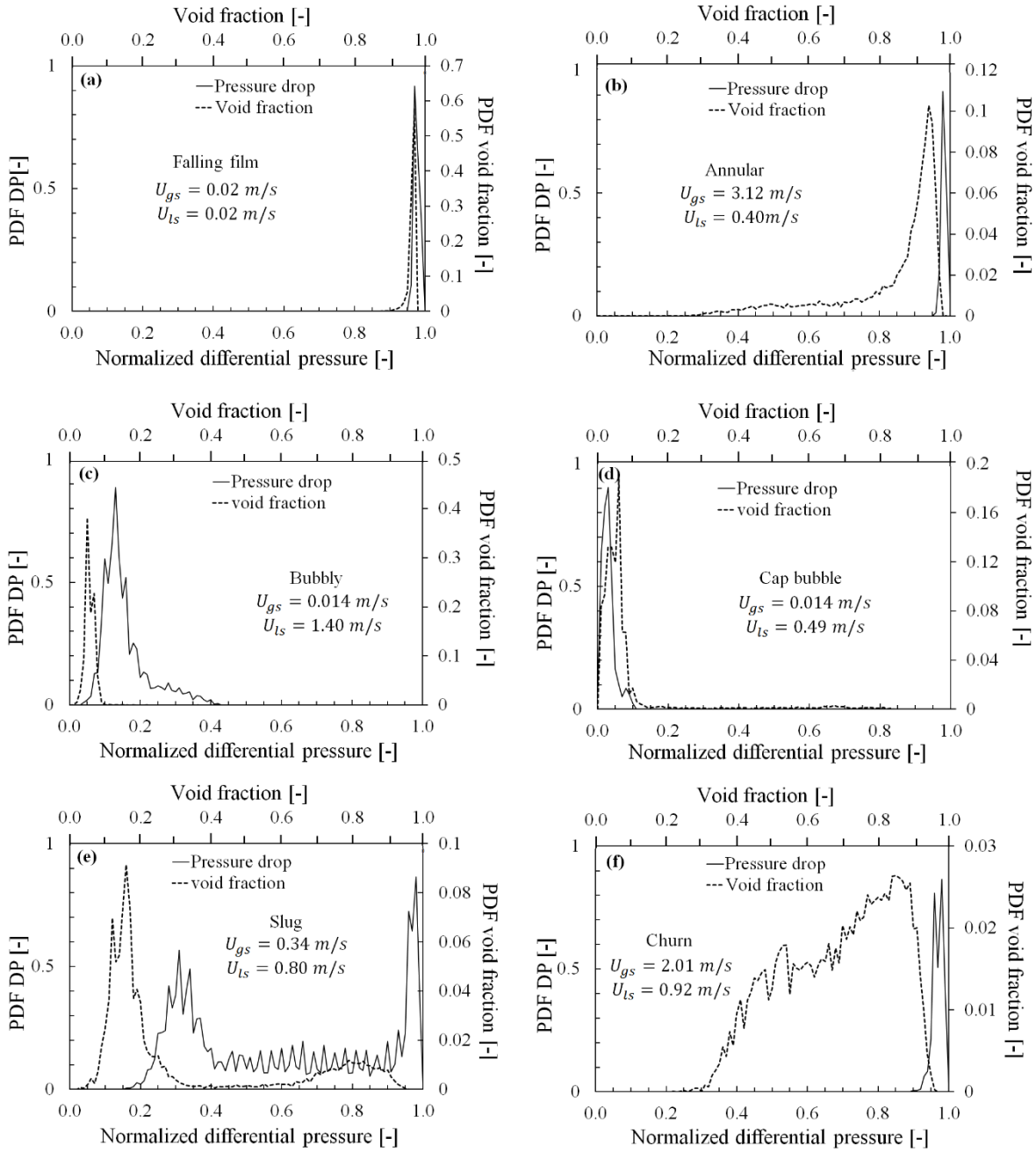

.

Fig. 8. Examples of PDFs of the normalized pressure drop and void fraction time series.

4.4 Flow pattern map

The experimentally observed flow regimes are represented in a flow map using mixture Froude number, Fr_M, and the ratio of gas-to-liquid superficial velocities, U_{gs}/U_{ls}, as coordinates. The result is depicted in Fig. 9. The mixture Froude number, given by Eq. 14, is used to normalize the mixture velocity, U_M, which is the sum of gas and liquid superficial velocities (Eq. 15).

$$Fr_M = \sqrt{\frac{\rho_l}{\rho_l - \rho_g}} \frac{U_M}{\sqrt{gD}} \tag{14}$$

$$U_M = U_{gs} + U_{ls} \tag{15}$$

Figure 9 shows clearly that the data of each flow pattern is presented in a specific region. The Falling film, and annular flow patterns are the dominant regimes, occupying wide ranges of Froude number and U_{gs}/U_{ls}. The obtained lines separating each regime, drawn in the flow map, are the transition lines of the present experimental setup. The proposed flow map has the advantage of using dimensionless numbers as coordinates compare to the majority of existing ones, summarized in Table 1.

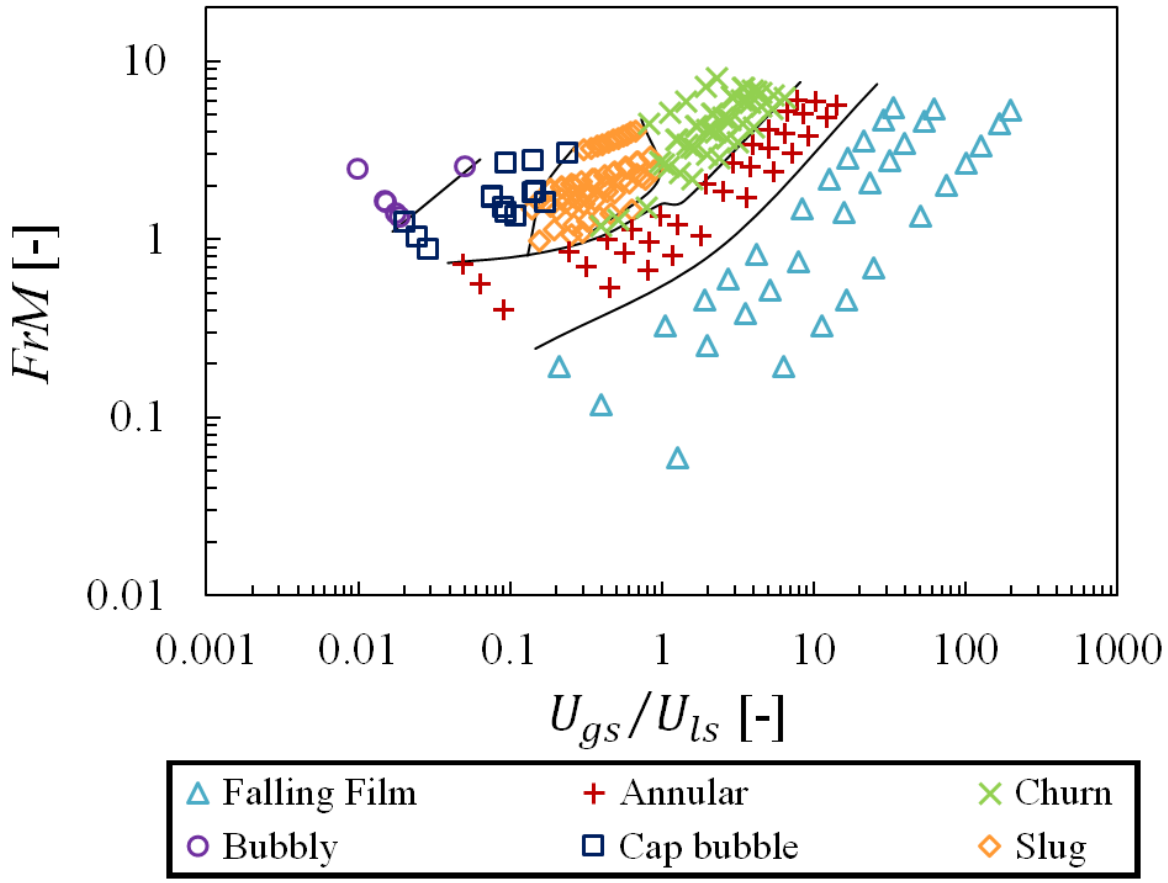

Fig. 9. Representation of flow pattern observed on flow map using Fr_M and U_{gs}/U_{ls} as coordinates

4.5 Mean void fraction

The void fraction refers to the section occupied by the gas to the total cross-sectional area. It is a crucial hydrodynamic parameter, particularly for vertical downward flows, which have not been extensively studied in literature. To gain more understanding in this area, we analyzed the temporal mean void fraction measured for all observed flow regimes. The values were obtained by averaging the recorded values during the acquisition.

In Fig. 10.a, the results of void fraction for different U_{ls} are shown as a function of U_{gs}. The plot reveals the presence of three distinct zones. In Zone I, an increase in U_{gs} leads to a

significant increase in the void fraction, while U_{ls} appears to have little effect in this zone. In Zone II, the void fraction increases due to the increase in gas superficial velocity and the decrease in liquid superficial velocity. On the other hand, in Zone III, the void fraction remains independent of U_{gs}.

Noting that the presence of three zones was already reported in the literature by Bhagwat and Ghajar (2012), Xue et al. (2016) and Chalgeri and Jeong (2019). The observed critical value to distinguish between zones II and III is the same as that reported by Bhagwat and Ghajar (2012) ($\varepsilon_G = 0.7$). Xue et al. (2016) have reported that this transition occurs at a greater value of the void fraction. Only the behavior of zone II is reported in vertical upward flow (Chalgeri and Jeong, 2019). This special feature of void fraction for downward flow constitutes additional evidence of the uniqueness of this flow configuration compared to upward flow.

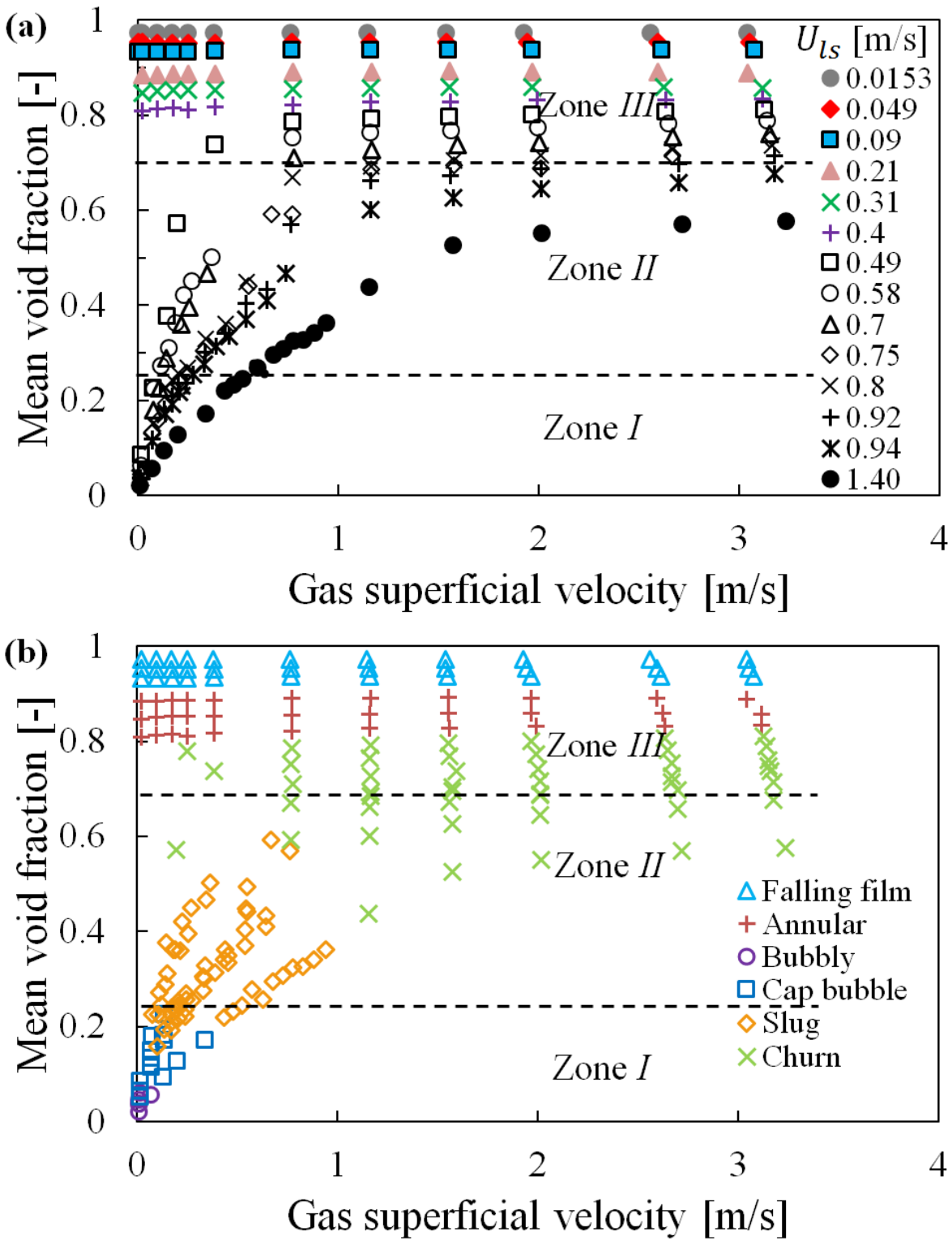

Fig. 10. Evolution of the void fraction function of the gas superficial velocity. (a) for different liquid superficial velocity and (b) for different flow patterns.

We also have analyzed the evolution of the void fraction based on the gas superficial velocities and flow regime nature (See Fig. 10.b). The analysis revealed a direct relationship between the flow regimes and the zones. Zone I comprises of data obtained from bubbly and cap bubble flows, with some data from slug flowas well. Zone II and III are occupied by slug flow and segregated flow data respectively. Note that segregated flow comprises both annular and falling film flows. The churn flow, which is a transition between slug and annular flow, occupies both latter zones.

The distribution of flow regimes in the three zones was also observed by Xue et al. (2016). However, they also reported the presence of churn and some points of annular flow in zone II. On the other hand, Bhagwat and Ghajar (2012) noted that Zone III is mainly occupied by annular and falling film flows. These discrepancies between the different studies can be attributed to the difference in pipe diameters, as well as the ranges of liquid and gas superficial velocities that were studied. It should be noted that Chalgeri and Jeong (2019) did not investigate the relationship between the three zones and the flow regimes.

Figure 11 shows the evolution of the mean void fraction measured for the 194 points as a function of the gas-to-liquid superficial velocities ratio. The latter was chosen as coordinate because it was demonstrated in the flow map (Fig. 9) that it is appropriated to model the transition between the six flow regimes. As already observed in Fig. 10.b, the void fraction is almost constant for each liquid superficial velocity value for falling film and annular flows. Fig. 11 highlights also that an increase of the gas-to-liquid superficial velocities ratio leads to a raise of the ratio of the surface occupied by the gas in the cross-section area of the pipe for the four other studied flow regimes. Focusing on the void fraction values obtained, it seems that the transition from bubbly to churn through, respectively, cap bubble and slug flows is accompanied by an increase of void fraction. The falling film and annular flows exhibit the

highest values of the mean void fraction ranging from $0.933 \leq \varepsilon_G \leq 0.973$ and $0.809 \leq \varepsilon_G \leq 0.892$, respectively.

The evolution of the homogenous void fraction or gas volumetric fraction ratio, β, given by Eq. 16, is also displayed in Fig. 11. It appears that the majority of the void fraction values are larger than the calculated homogenous void fraction. This case refers to the buoyancy-driven flow, according to Ghajar (2020). Note that except of bubbly and cap bubbly flow, other flow regimes exhibit the inertia-driven flow behavior ($\varepsilon_g < \beta$) for some superficial velocities ratio values.

$$\beta = \frac{U_{gs}}{U_M} \tag{16}$$

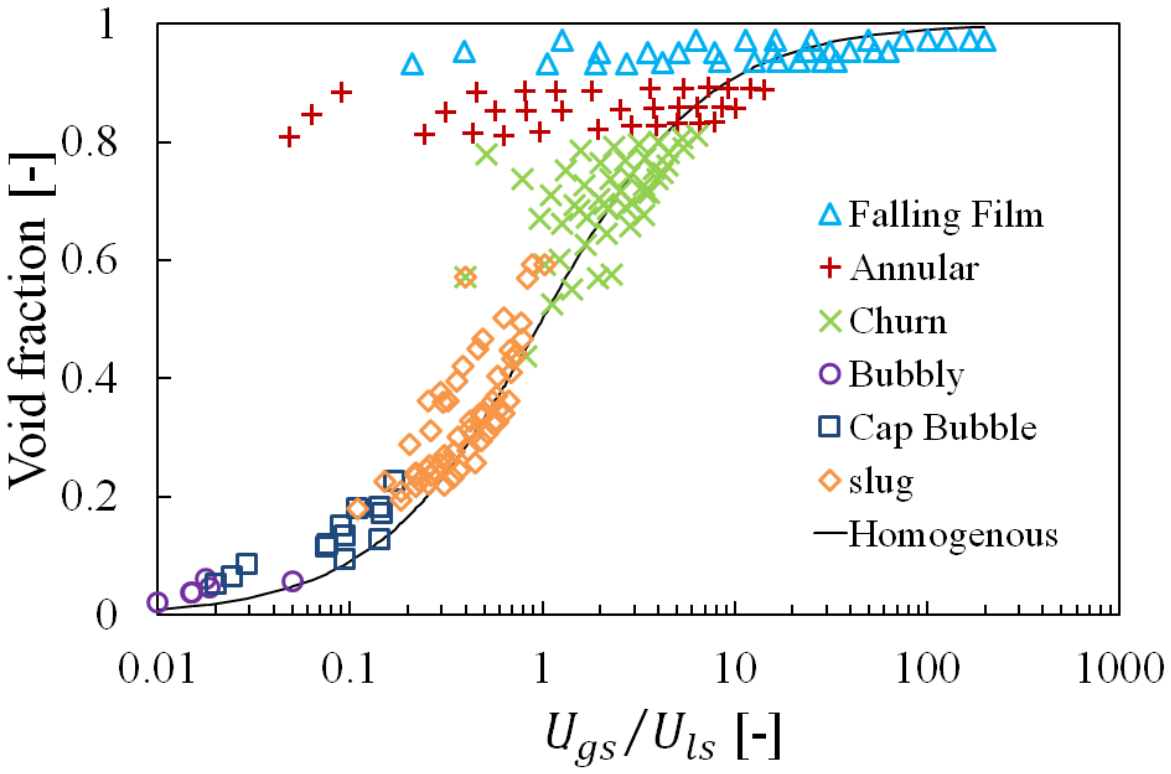

Fig. 11. Evolution of void fraction, ε_G, in function of U_{gs}/U_{ls} and comparison with the homogenous void fraction.

4.6 Total pressure drop

Figure 12 presents the measured total pressure drop versus gas superficial velocity. For better visibility, the data obtained in falling film and annular are represented separately (Fig. 12.a and 12.b, respectively). The rest of the data are plotted for each superficial liquid velocity (Fig. 12.c-f). Fig. 12.a depicts the results obtained with falling film and it shows the presence of three zones. For $U_{gs} \leq 0.096$ m/s, the increase of superficial gas velocity induces a decrease of total pressure drop. In the zone of intermediate values of superficial gas velocities, the total pressure drop increase with the increase of the latter until it becomes relatively constant. The annular flow exhibits also three zones, as it appears in Fig. 12.b. Indeed, it was observed successively the increase, decrease and relative stabilization of the total frictional pressure drop with the increase of the gas flow rate. It seems important to relativize the observed behavior knowing the low values of the collected total pressure drop for these two segregated flows.

Concerned the data obtained with the dispersed (bubbly and cap bubble), slug and churn flow regimes, we can observe that an increase of superficial gas velocity, for each value of superficial liquid velocity, induces a diminution of the total pressure drop for bubbly, cap bubble and slug flows. The transition of the churn flow is accompanied by a stabilization of the value of this parameter. We can note that Lu et al. (2018) reported also that an increase of superficial gas velocity induces a decrease of the total pressure drop for bubbly, cap bubble and slug flows.

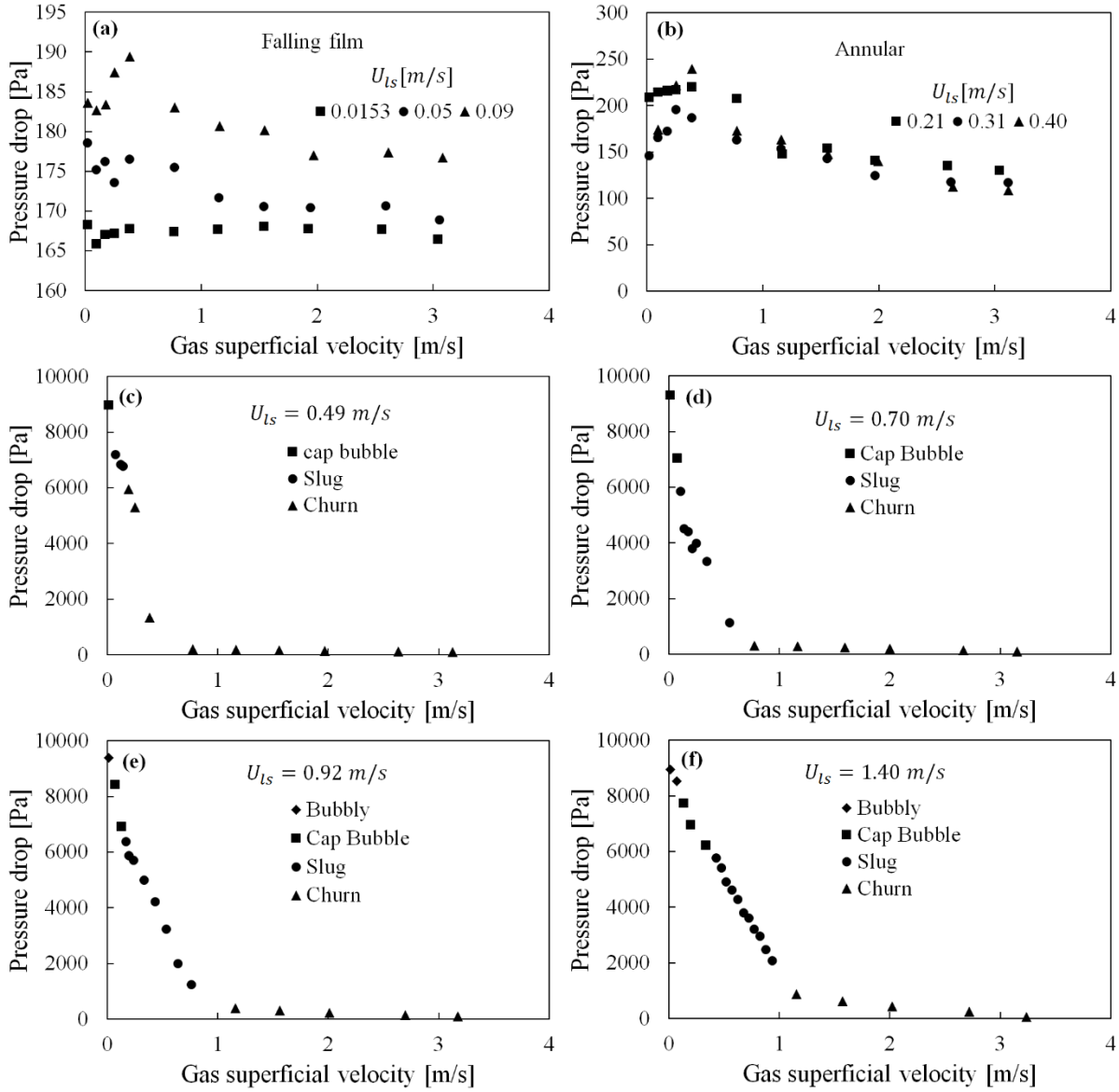

Fig. 12. Evolution of total pressure drop in function of superficial gas velocity and for different superficial liquid velocities and flow patterns

4.7 Frictional pressure drop

The frictional pressure drop are calculated utilizing Eqs. 1, 3 and 4. The frictional pressure drop is plotted as a function of the gas superficial velocity in Fig. 13. One can see that for the falling film (Fig. 13.a) and for U_{ls} = 0.05 and 0.09 m/s, the increase of superficial gas velocity induces an increase of frictional pressure drop before a decrease. For high values of U_{gs}, the frictional

pressure drop is not influenced by the latter. For the case of $U_{ls} = 0.015$ m/s, it seems that the gas superficial velocity has no influence on the evolution of the frictional pressure drop. This parameter is influenced by the gas superficial velocity for annular flow only for U_{gs} less than ≈ 0.174 m/s as it appears in Fig. 13.b. For the four other observed regimes, we can observe that an increment of superficial gas velocity induces an increase of frictional pressure drop for bubbly and cap bubble flows. Its increment induces a decrease or stabilization of frictional pressure drop for churn flow. For the slug flow, it seems that an increase of superficial gas velocity induces successively an increase, a decrease and then an increase of pressure drop. Similar observations have been reported for slug flow by Bhagwat et al. (2012), while Yao et al. (2018) have observed only the first inflection point for some slug flow conditions. These discrepancies can be explained by the difference in the pipe diameter and the superficial velocities of the phases, investigated in each study.

As pointed by Yao et al. (2018), in the two-phase gas-liquid vertical downward flow, the buoyancy forces act on gas bubble in the opposite direction to the flow. The clustering of gas in form of Taylor bubble in the case of slug and churn flows has the effect of further decelerating the motion of gas bubbles. Knowing that both slug and churn flow have formed by the alternating flow of two hydrodynamic structures (Bouyahiaoui et al., 2018, 2020) and that the liquid is flowing faster than the ahead Taylor bubble, it is expected that the liquid flow will overtake the latter. This 'overtaking" will cause a further friction, resulting in an increase of the frictional pressure drop. Intuitively, it appears that this additional increase of the momentum is dependent on the liquid and gas bubble velocities and also on the length and the width of the gas bubble. The increase of the slug frequency leads also to promote the occurrence of this overtaking phenomenon. This phenomenon can be the reason to the behavior of frictional pressure drop with respect to U_{gs}.

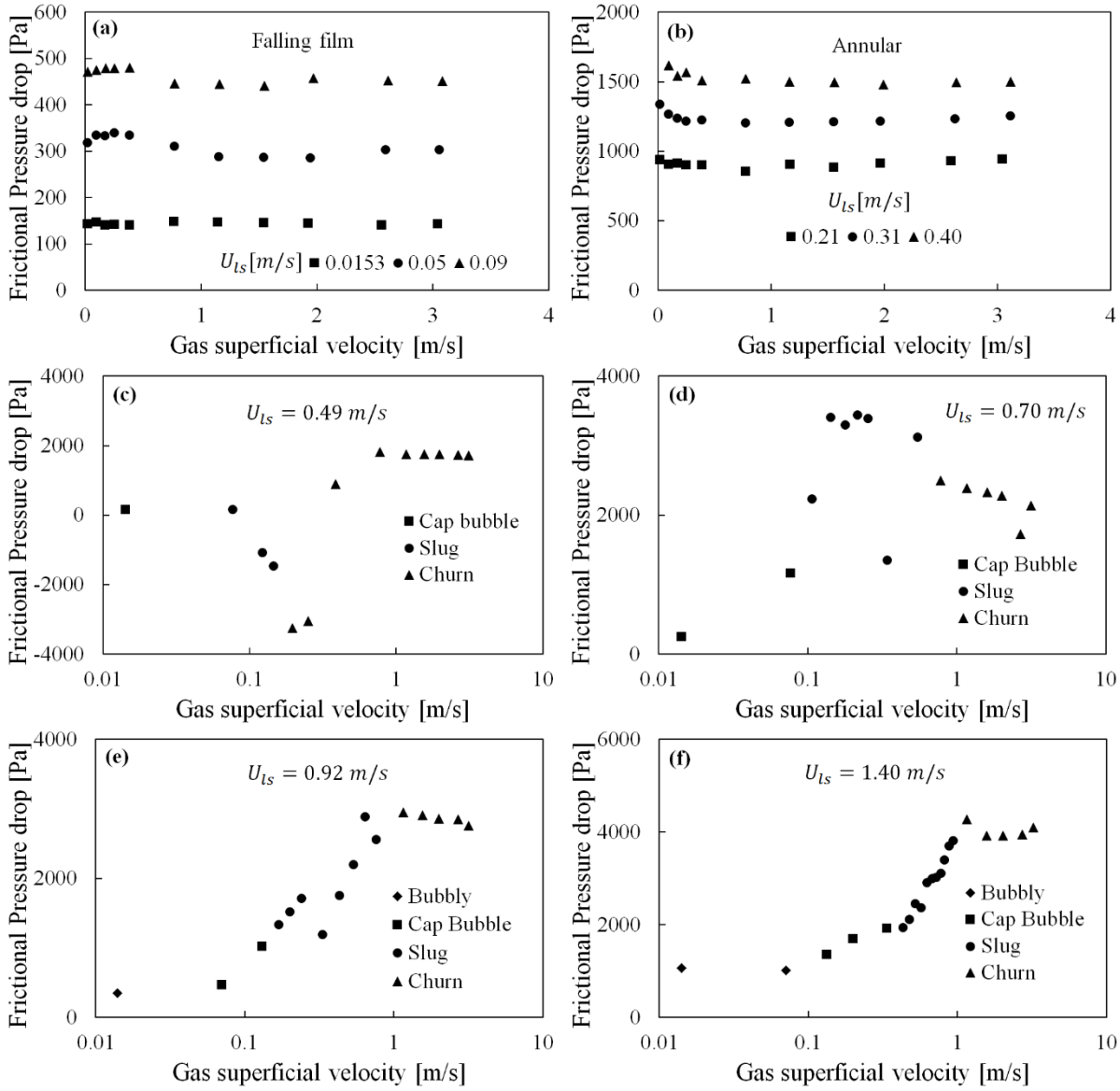

Fig. 13. Evolution of frictional pressure drop in function of gas superficial velocity and for different liquid superficial velocities and flow patterns.

It is also worth noting that we have observed a peculiar outcome that involves the presence of points in instances where the calculated frictional pressure drop is less than zero. This unusual behavior has only been reported in the cases of slug and churn, and it appears to occur solely when the liquid superficial velocities are at 0.49 and 0.58 m/s.

Al-sarkhi et al. (2016a) studied in detail the negative pressure drop phenomenon and explained the reason for that. The authors first made a literature survey on studies that reported this phenomenon when only experimental investigations carried out on vertical upward flow were reported. After, the authors modeled the wall shear stress in the Taylor bubble and the liquid slug zones to explain the root cause of this phenomenon.

According to Al-Sarkhi et al. (2016a), the total wall shear stress in the slug unit is the addition of two opposite wall shear stresses. The one generated by the liquid film upward, driven by the buoyancy of Taylor bubbles and that provoked by the liquid slugs flows in the direction of the flow. The positive or negative values of the pressure drop depends on the magnitude of these two opposite shear stresses. The fact that the negative pressure drop is observed in the present study only for the slug and churn flows can only confirm the validity of the explanation of Al-Sarkhi et al. (2016a) for vertical downward flow. The presence of both inertia-driven and buoyancy-driven flows behavior for slug and churn flows, noted in Section 4.5, reinforces this explanation. Note that the points of churn flow when negative pressure drop was reported are close to the slug-to-churn transition.

4.8 Comparison of frictional pressure drop with existing models

In this section, the experimental results of frictional pressure drop obtained in this study are compared with the predictions given by the four existing models developed for vertically downward flow; namely the model of Yamazaki and Yamaguchi (1979), Friedel (1979), Yao et al. (2018) and Lu et al. (2018). For this purpose, we have used two parameters which are the mean absolute relative deviation (*MARD*) and the mean relative deviation (*MRD*) The two parameters are expressed by Eqs. 17 and 18, respectively.

$$MARD = \frac{1}{N}\sum_{i=1}^{N}\left|\frac{y(i)_{pred} - y(i)_{exp}}{y(i)_{exp}}\right| \quad (17)$$

$$MRD = \frac{1}{N}\sum_{i=1}^{N}\frac{y(i)_{pred} - y(i)_{exp}}{y(i)_{exp}} \quad (18)$$

which $y(i)_{pred}$ and $y(i)_{exp}$ are respectively the prediction and the experimental measured value of the ith experimental data point. A positive and negative value of *MRD* mean that the model overestimate and underestimate, respectively, the experimental results.

The *MARD* and *MRD* calculated for each model and each flow regime are summarized in Table 4. Note that the data when negative frictional pressure drop are collected have not been considered in the assessment study. The first observation that emerge from this table is that the predictions of each model depend greatly on the nature of the flow pattern. The most remarkable example is observable with both segregated flows. Indeed, with *MARD* = 141.80 % and *MRD* = 109.74 %, the model of Yao et al. (2016) has largely overestimated the data collected for annular, meanwhile, it has underestimated the experimental results obtained with the falling film (*MARD*= 104.60 % and *MRD* = -71.81 %).

Table 4. Performance evaluation of the existing correlations against the experimental data. The results are given in %.

	Yamazaki and Yamaguchi (1979)		**Friedel (1979)**		**Yao et al. (2016)**		**Lu et al. (2018)**	
	MARD	***MRD***	***MARD***	***MRD***	***MARD***	***MRD***	***MARD***	***MRD***
Falling film	84.72	-84.72	83.26	-83.26	104.60	-71.81	**75.96**	**-75.95**
Annular	78.50	-78.50	75.30	-75.30	141.80	109.74	**69.95**	**-69.95**
Bubbly	37.52	-37.52	29.53	**-29.53**	37.79	-37.79	**25.85**	**-25.08**
Cap bubble	54.12	-54.12	41.56	-41.56	57.80	-57.80	**40.02**	**-40.03**
Slug	72.16	-72.16	**62.55**	**-61.83**	68.32	-30.42	65.43	-64.51
Churn	55.40	-55.40	51.46	-51.46	**38.03**	**35.22**	44.37	-44.37
All database	68.89	-68.89	63.02	-62.81	78.02	-0.04	**59.74**	**-59.44**

*** the best predictions for each database is written in bold.**

Evaluating the prediction models for each flow regime, it has been observed that the model by Lu et al. (2018) is the most accurate in predicting the results for falling film, annular, bubbly, and cap bubble flows. However, it is important to note that both statistical parameter values for segregated flows are high. For bubbly flow, the model by Friedel (1979) and Lu et al. (2018) predicted the data with a similar order of magnitude. Additionally, the values of *MARD* and *MRD* for bubbly flow are the only ones those are below 30%.

The model of Friedel (1979) is the model that gives the best prediction of the slug flow experimental results, noting that the considerable (high) values of *MARD* and *MRD* (62.55% and -61.83%, respectively). The model of Yao et al. (2016), which takes into account the

buoyancy forces give the best prediction with the data collected for churn flow. The fact that the model of Lu et al. (2018) is the model that best predict four out of the six regimes ensures that it gives the best prediction of all database. Noting that the important value of *MARD* (59.74%) as well as the recorded *MRD* values are negatives and their absolute values are equal to the *MARD* values for almost the whole database (except for slug flow). These observations mean that the models have underestimated the whole experimental database for five flow regimes.

Figure 14 represents a graphical plot used for the assessment evaluation of the four models. The diagonal line as well as the deviation bands of -30 % and +30% are also displayed in the figure.

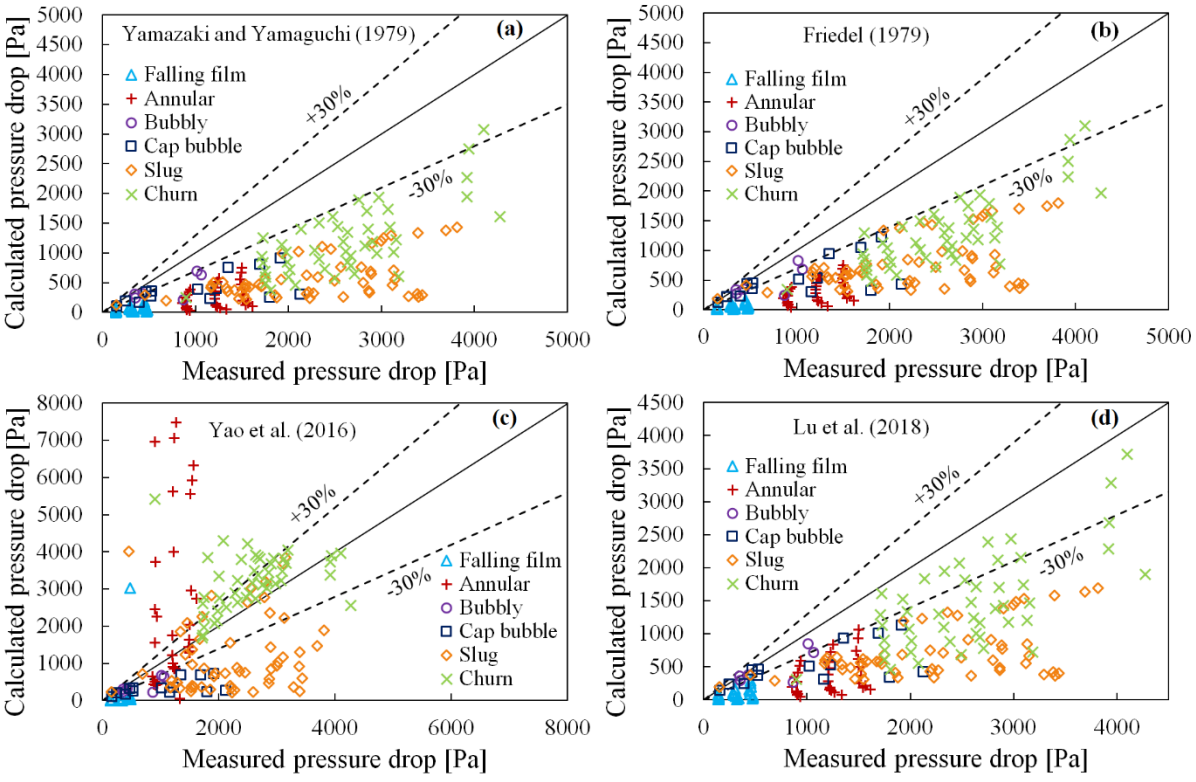

Fig. 14. Comparison between the prediction of the existing predictive models and the experimental results.

For the model of Yamazaki and Yamaguchi (1979), it appears clearly from Fig. 14.a that the model highly underestimates the experimental results for all the six regimes. Only few points are above the line of -30%. The same observation is also valid for the model of Friedel (1979) (Fig. 14.b). A deep observation of the plot shows that this model gives acceptable results for the low experimental values recorded with bubbly and cap bubble. Referring to what is explained in section 4.7, this low value refers to the low values of gas and liquid superficial velocities. The comparison of the experimental results with the prediction of the model of Yao et al. (2016), depicted in Fig. 14c, shows that this model is the model that gives the most important scatterings of the results. It is also the model that the most results within ±30% have been obtained. From Fig. 14.d, it appears that the model of Lu et al. (2018) predicts the acquired data satisfactorily at low superficial velocities of both phases for dispersed flow.

This analysis shows that no model developed for vertical downward flow can predict satisfactorily the entire database. In addition, except for bubbly flow regime with the models of Friedel (1979) and Lu et al. (2018), no *MARD* values less than 30% have been recorded. This shows the difficulty of predicting the pressure drop for this geometry and the necessity of proposing a new model.

5. Conclusions

This study aims to investigate experimentally the vertical downward gas-liquid two-phase flows. For this purpose, experiments were carried out in order to collect a total of 194 database of mean void fraction and pressure drop corresponding to different values of gas and liquid superficial velocities. For the experimental conditions investigated, a total of six flow regimes were observed. The conclusions drawn from this study can be summarized as:

- The analysis of the time series of void fraction and pressure drop allowed to observe that the obtained signals are specific for each flow pattern. The utilization of the PDF as a tool to identify and distinct between the flow regimes is shown. The results seem more interesting with the void fraction time series than the pressure drop time series.
- A new flow pattern map was proposed for the used pipe diameter. This flow pattern uses the mixture Froude number and the ratio of gas-to-liquid superficial velocities as coordinates.
- The influence of both liquid and gas superficial velocities on the mean void fraction was found to depend on the flow regime.
- Similar to void fraction, the behaviors of total and frictional pressure drop with the gas and liquid superficial velocities depend on the nature of the flow regime.
- For some cases, the phenomenon of negative frictional pressure drop was observed. The analogy with the explanation made by Al-sarkhi et al. (2016a) for the case of vertical upward flow allowed to explain this phenomenon.
- The prediction of the four existing frictional pressure drop models developed for the vertical downward flow are evaluated with the present experimental data. The comparison showed that none of the models can predict accurately the experimental results. Additionally, the prediction of each model was found to be dependent on the nature of the flow regime.
- In addition to the generated database of void fraction and pressure drop which can be used to develop more robust and efficient predictive models as well as for the validation of simulations obtained using CFD. The paper has allowed to bring into the surface the great influence of the flow regime on the studied parameters. It is strongly recommended to conduct additional studies to understand flow behavior and transitions and to generate more databases.

References

Abdulkadir, M., Kajero, O. T., O Olarinoye, F., O Udebhulu, D., Zhao, D., Aliyu, A. M., & Al-Sarkhi, A., 2021. Investigating the Behaviour of Air–Water Upward and Downward Flows: Are You Seeing What I Am Seeing?. Energies, 14(21), 7071. https://doi.org/10.3390/en14217071

Abdulkadir, M., Jatto, D. G., Abdulkareem, L. A., & Zhao, D., 2020. Pressure drop, void fraction and flow pattern of vertical air–silicone oil flows using differential pressure transducer and advanced instrumentation. Chemical Engineering Research and Design. 159, 262-277. https://doi.org/10.1016/j.cherd.2020.04.009

Al-Sarkhi, A., Pereyra, E., Sarica, C., & Alruhaimani, F., 2016a. Positive frictional pressure gradient in vertical gas-high viscosity oil slug flow. International Journal of Heat and Fluid Flow, 59, 50-61. https://doi.org/10.1016/j.ijheatfluidflow.2016.01.008

Al-sarkhi, A., Sarica, C., & Pereyra, E., 2016b. New dimensionless number for gas–liquid flow in pipes. International Journal of Multiphase Flow. 81, 15-19. https://doi.org/10.1016/j.ijmultiphaseflow.2015.12.008

Arabi, A., Saidj, F., Al-Sarkhi, A., & Azzi, A., 2022. Analogy between Vertical Upward Cap Bubble and Horizontal Plug Flow. SPE Journal. 1-20. https://doi.org/10.2118/209235-PA

Arabi, A., Zenati, Y., Si-Ahmed, E. K., & Legrand, J., 2023. Identifying the intermittent flow sub-regimes using pressure drop time series fluctuations. Accepted for publication in Experimental and Computational Multiphase Flow. Preprint available at ResearchSquare. https://doi.org/10.21203/rs.3.rs-2510593/v1

Barnea, D., Shoham, O., & Taitel, Y., 1982. Flow pattern transition for vertical downward two- phase flow. Chemical Engineering Science. 37(5), 741-744. https://doi.org/10.1016/0009-2509(82)85034-3

Bhagwat, S. M., Mollamahmutoglu, M., & Ghajar, A. J., 2012, July. Experimental investigation and performance evaluation of isothermal frictional two phase pressure drop correlations in vertical downward gas-liquid two phase flow. In Heat Transfer Summer Conference (Vol. 44786, pp. 337-348). American Society of Mechanical Engineers. https://doi.org/10.1115/HT2012-58049

Bhagwat, S. M., & Ghajar, A. J., 2017. Experimental investigation of non-boiling gas-liquid two phase flow in downward inclined pipes. Experimental Thermal and Fluid Science. 89, 219-237. https://doi.org/10.1016/j.expthermflusci.2017.08.020

Bouyahiaoui, H., 2019. Analyse Hydrodynamique d'un Écoulement Diphasique Gaz-liquide Descendant (Doctoral dissertation, Université des Sciences et de la Technologie d'Alger, Houari Boumediène).

Bouyahiaoui, H., Azzi, A., Zeghloul, A., Hasan, A. H., Al-Sarkhi, A., & Parsi, M., 2020. Vertical upward and downward churn flow: Similarities and differences. Journal of Natural Gas Science and Engineering. 73, 103080. https://doi.org/10.1016/j.jngse.2019.103080

Bouyahiaoui, H., Azzi, A., Zeghloul, A., Hasan, A., & Berrouk, A. S., 2018. Experimental investigation of a vertically downward two-phase air-water slug flow. Journal of Petroleum Science and Engineering. 162, 12-21. https://doi.org/10.1016/j.petrol.2017.12.028

Chalgeri, V. S., & Jeong, J. H., 2022. Flow regime transition criteria for vertical downward two-phase flow in rectangular channel. Nuclear Engineering and Technology. 54(2), 546-553. https://doi.org/10.1016/j.net.2021.08.014

Cherdantsev, M. V., Isaenkov, S. V., Cherdantsev, A. V., & Markovich, D. M., 2021. Development and interaction of disturbance waves in downward annular gas-liquid flow. International Journal of Multiphase Flow. 138, 103614. https://doi.org/10.1016/j.ijmultiphaseflow.2021.103614

Costigan, G., & Whalley, P. B., 1997. Slug flow regime identification from dynamic void fraction measurements in vertical air-water flows. International Journal of Multiphase Flow. 23(2), 263-282. https://doi.org/10.1016/S0301-9322(96)00050-X

Friedel, L., 1979. Improved friction pressure drop correlations for horizontal and vertical two-phase pipe flow. In European Two-Phase Flow Group Meeting. Ispra, Italy.

Ghajar, A. J., 2022. Single-and Two-Phase Flow Pressure Drop and Heat Transfer in Tubes. Springer Nature Switzerland. Switzerland. ISBN: 978-3-030-87281-6

Ghajar, A. J., & Bhagwat, S. M., 2014. Flow patterns, void fraction and pressure drop in gas-liquid two phase flow at different pipe orientations. In Frontiers and Progress in Multiphase Flow I (pp. 157-212). Springer, Cham. DOI: 10.1007/978-3-319-04358-6_4

Goda, H., Hibiki, T., Kim, S., Ishii, M., & Uhle, J., 2003. Drift-flux model for downward two-phase flow. International journal of heat and mass transfer. 46(25), 4835-4844. https://doi.org/10.1016/S0017-9310(03)00309-0

Guo, W., Liu, C., & Wang, L., 2021. Temperature fluctuation on pipe wall induced by gas–liquid flow and its application in flow pattern identification. Chemical Engineering Science. 237, 116568. https://doi.org/10.1016/j.ces.2021.116568

Hajiloo, M., Chang, B. H., & Mills, A. F., 2001. Interfacial shear in downward two-phase annular co-current flow. International journal of multiphase flow. 27(6), 1095-1108. https://doi.org/10.1016/S0301-9322(00)00065-3

Hammer, M., Deng, H., Liu, L., Langsholt, M., & Munkejord, S. T., 2021. Upward and downward two-phase flow of CO2 in a pipe: Comparison between experimental data and model predictions. International Journal of Multiphase Flow. 138, 103590. https://doi.org/10.1016/j.ijmultiphaseflow.2021.103590

Hernandez, A., Gonzalez, L., & Gonzalez, P., 2002, September. Experimental research on downward two-phase flow. In SPE Annual Technical Conference and Exhibition. OnePetro. https://doi.org/10.2118/77504-MS

Ishii, M., Paranjape, S. S., Kim, S., & Sun, X., 2004. Interfacial structures and interfacial area transport in downward two-phase bubbly flow. International journal of multiphase flow. 30(7-8), 779-801. https://doi.org/10.1016/j.ijmultiphaseflow.2004.04.009

Kang, J., Zhang, X., Zhang, D., & Liu, Y., 2021. Pressure drops and mixture friction factor for gas–liquid two-phase transitional flows in a horizontal pipe at low gas flow rates. Chemical Engineering Science. 246, 117011. https://doi.org/10.1016/j.ces.2021.117011

Kim, T. H., Chalgeri, V. S., Yoon, W., Yun, B. J., & Jeong, J. H., 2018. Visual observations of flow patterns in downward air-water two-phase flows in a vertical narrow rectangular channel. Annals of Nuclear Energy. 114, 384-394. https://doi.org/10.1016/j.anucene.2017.12.053

Lau, V., & Rezkallah, K. S., 1995. New data on two-phase water-air hydrodynamics in vertical upward and downward tubes. Wight, A.L.; Loewer, R. (eds.); Canadian Nuclear Society, 16. Annual conference of the Canadian Nuclear Society; Saskatoon, SK (Canada); 4-7 Jun 1995.

Lee, J. Y., Ishii, M., & Kim, N. S., 2008. Instantaneous and objective flow regime identification method for the vertical upward and downward co-current two-phase flow. International Journal of Heat and Mass Transfer. 51(13-14), 3442-3459. https://doi.org/10.1016/j.ijheatmasstransfer.2007.10.037

Li, Z., Wang, G., Yousaf, M., Yang, X., & Ishii, M., 2018. Flow structure and flow regime transitions of downward two-phase flow in large diameter pipes. International Journal of Heat and Mass Transfer. 118, 812-822. https://doi.org/10.1016/j.ijheatmasstransfer.2017.11.037

Liu, W., Xu, Q., Zou, S., Chang, Y., & Guo, L., 2021. Optimization of differential pressure signal acquisition for recognition of gas–liquid two-phase flow patterns in pipeline-riser system. Chemical Engineering Science. 229, 116043. https://doi.org/10.1016/j.ces.2020.116043

Liu, L., Huang, N., & Liu, D., 2022a. Divergency and consistency between frictional pressure drops from momentum balance and energy balance for two-phase flow. Chemical Engineering Science. 247, 117070. https://doi.org/10.1016/j.ces.2021.117070

Liu, W., Lv, X., Jiang, S., Li, H., Zhou, H., & Dou, X., 2023. Gas–liquid two-phase flow patterns and pressure drop of decaying swirling flow inside a horizontal pipe. Chemical Engineering Science. 266, 118281. https://doi.org/10.1016/j.ces.2022.118281

Lu, C., Kong, R., Qiao, S., Larimer, J., Kim, S., Bajorek, Tien, K. & Hoxie, C., 2018. Frictional pressure drop analysis for horizontal and vertical air-water two-phase flows in different pipe sizes. Nuclear Engineering and Design. 332, 147-161. https://doi.org/10.1016/j.nucengdes.2018.03.036

Lu, P., Ye, Q., Fang, L., Yang, P., & Yang, Q., 2021. Research on the air–oil two-phase flow regime in an aeroengine bearing chamber based on Hilbert–Huang transform. Proceedings of the Institution of Mechanical Engineers, Part G: Journal of Aerospace Engineering, 09544100211002956. doi/pdf/10.1177/09544100211002956

Matsui, G., 1984. Identification of flow regimes in vertical gas-liquid two-phase flow using differential pressure fluctuations. International journal of multiphase flow. 10(6), 711-719. https://doi.org/10.1016/0301-9322(84)90007-7

Passoni, S., Carraretto, I. M., Mereu, R., & Colombo, L. P. M., 2023. Two-phase stratified flow in horizontal pipes: a CFD study to improve prediction of pressure gradient and void fraction. Chemical Engineering Research and Design. https://doi.org/10.1016/j.cherd.2023.01.016

Qiao, S., Mena, D., & Kim, S., 2017. Inlet effects on vertical-downward air–water two-phase flow. Nuclear Engineering and Design. 312, 375-388. https://doi.org/10.1016/j.nucengdes.2016.04.033

Saidj, F., Kibboua, R., Azzi, A., Ababou, N., & Azzopardi, B. J., 2014. Experimental investigation of air–water two-phase flow through vertical 90° bend. Experimental thermal and fluid science. 57, 226-234. https://doi.org/10.1016/j.expthermflusci.2014.04.020

Santana, A. L. B., dos Santos, E. N., Alves, R. F., Bertoldi, D., da Silva, M. J., Neto, M. A. M., & Morales, R. E., COB-2021-1415 Experimental analysis of downward vertical air-water annular flow. ABCM, November, 22-26, 2021, Virtual Congress, Brazil.

Schmid, D., Verlaat, B., Petagna, P., Revellin, R., & Schiffmann, J., 2022. Flow pattern observations and flow pattern map for adiabatic two-phase flow of carbon dioxide in vertical upward and downward direction. Experimental Thermal and Fluid Science. 131, 110526. https://doi.org/10.1016/j.expthermflusci.2021.110526

Usui, K., 1989. Vertically downward two-phase flow,(II) Flow regime transition criteria. Journal of Nuclear Science and Technology. 26(11), 1013-1022. https://doi.org/10.1080/18811248.1989.9734422

Usui, K., & Sato, K., 1989. Vertically downward two-phase flow, (I) Void distribution and average void fraction. Journal of Nuclear Science and Technology. 26(7), 670-680. https://doi.org/10.1080/18811248.1989.9734366

Voulgaropoulos, V., Patapas, A., Lecompte, S., Charogiannis, A., Matar, O. K., De Paepe, M., & Markides, C. N., 2021. Simultaneous laser-induced fluorescence and capacitance probe measurement of downwards annular gas-liquid flows. International Journal of Multiphase Flow. 142, 103665. https://doi.org/10.1016/j.ijmultiphaseflow.2021.103665

Xue, Y., Li, H., Sheng, T., & Liao, C., 2013, July. Experimental investigation on flow patterns and frictional pressure drop of downward air-water two-phase flow in vertical pipes. In Heat Transfer Summer Conference (Vol. 55485, p. V002T07A003). American Society of Mechanical Engineers. https://doi.org/10.1115/HT2013-17230

Yamazaki, Y. and Yamaguchi, K., 1979. Characteristics of co-current two-phase downflow in tubes. Journal of Nuclear Sciences and Technology. 16(4), 245-255. DOI 10.3327/jnst.16.245

Yao, C., Li, H., Xue, Y., Liu, X., & Hao, C., 2018. Investigation on the frictional pressure drop of gas liquid two-phase flows in vertical downward tubes. International Communications in Heat and Mass Transfer. 91, 138-149. https://doi.org/10.1016/j.icheatmasstransfer.2017.11.015

Zadrazil, I., Matar, O. K., & Markides, C. N., 2014. An experimental characterization of downwards gas–liquid annular flow by laser-induced fluorescence: Flow regimes and film statistics. International Journal of Multiphase Flow. 60, 87-102. https://doi.org/10.1016/j.ijmultiphaseflow.2013.11.008

Zeghloul, A., Messilem, A., Ghendour, N., Al-Sarkhi, A., Azzi, A., & Hasan, A., 2021. Theoretical study and experimental measurement of the gas liquid two-phase flow through a vertical Venturi meter. Proceedings of the Institution of Mechanical Engineers, Part C: Journal of Mechanical Engineering Science. 235(9), 1567-1584. https://doi.org/10.1177/0954406220947118